



46<sup>TH</sup> TURBOMACHINERY & 33<sup>RD</sup> PUMP SYMPOSIA  
HOUSTON, TEXAS | DECEMBER 11-14, 2017  
GEORGE R. BROWN CONVENTION CENTER

## TORSIONAL EXCITATION UPON SHORT-CIRCUIT IN INDUCTION MOTORS - IN CONVENTIONAL AND HIGH-SPEED TRAINS -

### **Tuomo Aho**

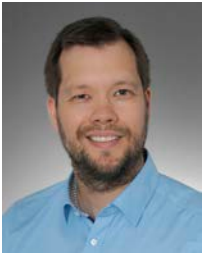
Electrical Engineering  
MAN Diesel & Turbo Schweiz AG  
Zürich, Switzerland

### **Christopher Baum**

Mechanical Development  
MAN Diesel & Turbo Schweiz AG  
Zürich, Switzerland

### **Janne Nerg**

Associate Professor D.Sc.  
Lappeenranta University of Technology  
Lappeenranta, Finland



*Tuomo Aho received his M.Sc. degree in Electrical Engineering from Lappeenranta University of Technology, Finland, in 2004. After continuing research work for development of the high-speed solid-rotor induction motors he received his D.Sc. degree from Lappeenranta University of Technology in 2007. During 2007-2010 he worked in Research and Development Department of Induction Motors at ABB Finland. Since 2010 he works for MAN Diesel & Turbo Schweiz AG and was active in Asgard Subsea Project during 2010-2014. Currently his job function in New Technologies team includes various research and development tasks for high-speed motors, but also supporting delivery projects as a technical responsible.*



*Christopher Baum graduated as Mechanical Engineer in 2011 at the University of Stuttgart (Germany). Since then he's active for MAN Diesel & Turbo Schweiz AG. His job function includes the development and analysis of components of centrifugal compressors for Oil & Gas applications. He is responsible for rotordynamics analysis of high speed and high pressure compressors as well as for mechanical stress analysis. Before joining the Mechanical Development Team his task was to perform mechanical and thermo-mechanical stress assessments for the Asgard Subsea Project.*



*Janne Nerg received the M. Sc. Degree in electrical engineering, the Licentiate of Science (Technology) degree, and the D. Sc. (Technology) degree from Lappeenranta University of Technology (LUT), Lappeenranta, Finland, in 1996, 1998, and 2000, respectively. He is currently an Associate Professor in the Department of Electrical Engineering at LUT. His research interests are in the field of electrical machines and drives, especially electromagnetic and thermal modeling and design of high-speed electrical machines.*



## ABSTRACT

In recent years more and more gas compressor trains are driven by a Variable Frequency Drive (VFD) instead of a gas turbine. One of the most common electric faults of the electric motor is short-circuit. Even though this can lead to catastrophic damage, too often the short-circuit analysis for VFD supplied motors is neglected in contrast to Direct On-Line (DOL) motors – assuming that the short-circuit torque is limited by the fast reaction of the VFD and its protection functions. Since the short-circuit current and the resulting electromagnetic torque is limited solely by a short-circuit impedance of the motor, not by the VFD, short-circuit load cases have to be analyzed during the design phase.

In this paper calculation of the short-circuit excitation torque when the induction motor is either DOL connected or connected to a VFD is discussed. A focus is put on the high-speed applications, especially on the high-speed solid-rotor induction motors. Differences between different calculation methods for excitation torque calculation are discussed. Influence of the equivalent circuit parameters on the motor short-circuit behavior is explained. Analytical and FEM methods for analyzing the excitation torque are presented.

Furthermore the influence on the mechanical torsional rotordynamic system is shown. Modelling and parameters of the torsional calculation are discussed. A comparison of different train configurations shows the different design considerations that need to be taken into account. Methods to evaluate and tune the rotordynamics of the train system with respect to shear stresses, amplification factors and torsional natural eigenfrequencies are given.

## INTRODUCTION

The popularity of gas compressor trains driven by a VFD instead of a gas turbine has increased in recent years. The increased speed and process flexibility comes at cost of increased electrical and mechanical complexity. Various authors have shown the impact of torque ripple contents, interharmonics (Hütten et al. 2008) and white noise (Kocur and Muench 2011) on the torsional system behavior and mechanical integrity of the system. The most common electric motor fault – the short circuit – affects the whole drive train. Short-circuits in motor winding insulation (e.g. Figure 1 left), in its power cabling or in the power supply system, can result in high transient torques in the motor shaft which can potentially excite torsional modes in the drive train and create high loads on the coupling and the motor foundation. This can lead to catastrophic damages.

Corcoran et al. (2010) have shown that VFDs play a crucial role when it comes to coupling failures (e.g. Figure 1 middle/right). Careful machine layout with consideration of transient torques resulting from short-circuits is necessary to protect personnel and apparatus. Special considerations are also required in order to limit the excessive transient electrical short-circuit power in the motor winding, in the power supply cables and in the power supply system.



Figure 1: Fault of Stator Winding (Karmakar et al. 2016) / Coupling Failures (Corcoran et al. 2010).

This paper treats torsional excitation torques upon short-circuit incidents in electric motor driven compressor trains, with primary focus on integrated high-speed induction motor-compressors. A comparison to a conventional trains composed of a motor connected to a compressor via a speed increasing gearbox is made. Short-circuit characteristics of high-speed motors are derived and a transient torsional analysis of a compressor train is performed. Methods to calculate and evaluate fatigue stress limits are shown and explained. Particular parts of interest such as couplings and bolts are highlighted and analyzed. As the impact of short-circuits on specific train affects a-priori unknown critical sections, the identification of the most critical load cases is explained.



## COMPRESSOR TRAIN ARRANGEMENTS

Traditional compressor trains are composed of a compressor, a speed increasing gearbox and an electric motor. Shaft connections between motor, gearbox and compressors are either realized with flexible or rigid couplings. Depending on the application, supplying electric grid and constraints set by an operator and specifications, electric motors can be either Direct On-Line (DOL) connected as shown in Figure 2 or supplied by a VFD respectively.

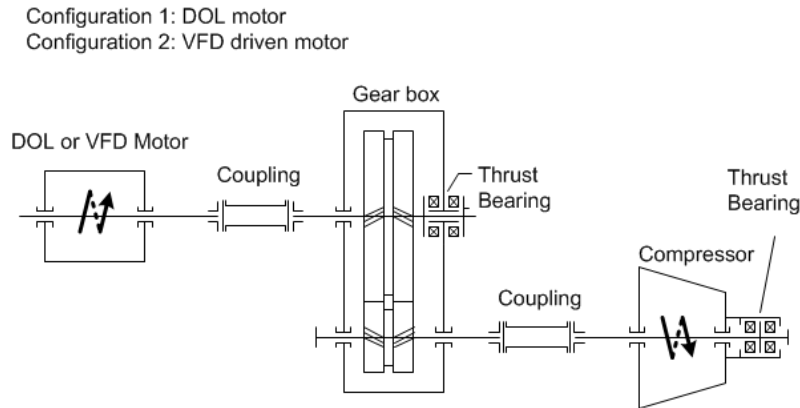


Figure 2: Configurations 1 and 2: Compressor, a Speed Increasing Gear Box and a Direct On-Line Motor or Variable Frequency Driven Motor.

As opposed to the traditional configurations, a high-speed electric motor application can be used, where the electric motor shaft is directly connected to a compressor shaft with a coupling without a speed increasing gearbox (Figure 3). When compressors and motors in such trains operate at rotational speeds higher than allowed by the supplying electric power grid, i.e. over 3600 rpm (in 60 Hz network) or 3000 (in 50 Hz network) respectively, the use of a VFD is inevitable.

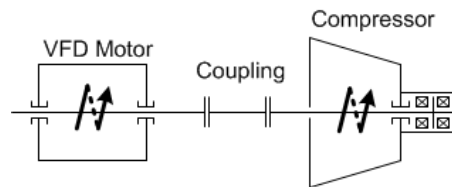


Figure 3: Configuration 3: Compressor, a High-Speed Motor supplied by a Variable Frequency Drive.

Even though the use of synchronous motors is theoretically possible, the electric motors for compressors in industrial use are commonly induction motors, also known as asynchronous motors.

## SHORT-CIRCUITS IN ELECTRICAL MACHINES

Even though an induction motor is rather robust motor type in its nature, there are several types of faults that may take place in induction motors. According to surveys made by IEEE (Grigg, et al. 1987), EPRI (Albrecht, 1986 and 1987) and later by (Thorsen and Dalva, 1995) and (Bonnett, 2010), approximately 40 % of all induction motor failures are caused by bearing faults, 35 % by stator faults, 10 % by rotor faults, and 15 % by miscellaneous faults. Stator faults in terms of winding insulation failure and miscellaneous faults taking place in the main terminal box of the motor can cause a short-circuit event. According to industrial surveys on the electrical machine reliability, the stator winding insulation is one of the most vulnerable components used in electrical machines. Stator faults are basically caused by a breakdown of winding insulation, which may result from thermal overheating, excessive voltage stress, mechanical vibration or even from rubbing of the rotor in the stator of the motor. Insulation breakdown and hence short-circuit



may be present between the electric conductors within the stator, which is called phase-to-phase short-circuit. It is also a possibility that the short-circuit takes place in the motor power cables or in the output of the power supply.

In general, it can be said, that short-circuit torque peak values are throughout the range from 3 to 15 times the rated full load-torque of the motor. Figure 4 shows short-circuit torque peak ratings observed by authors in the executed projects for conventional speed and high-speed induction motors used in oil and gas industry in the power range of 3-20 MW.

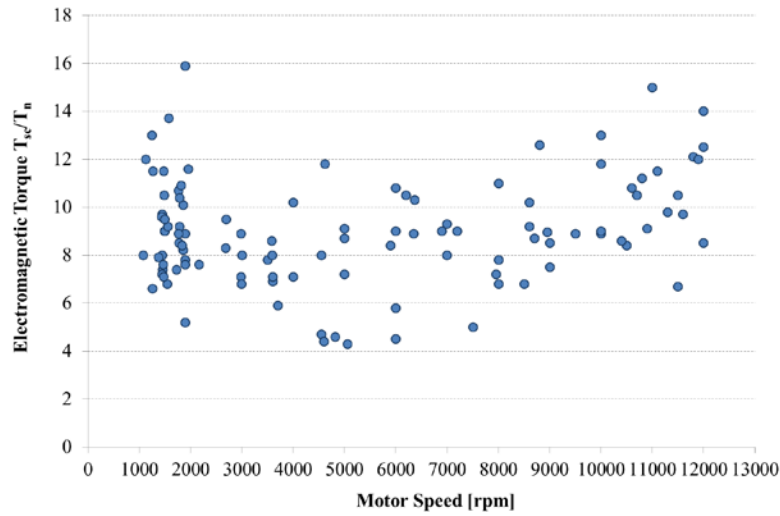


Figure 4: Short-Circuit Peak Torque Ratings for Induction Motors in Power Range of 3-20 MW Based on Authors' Experience in the Executed Projects.

In most of cases in industrial applications, an induction motor is connected Direct On-Line to a transformer. Short-circuit protection of electric motors is primarily based on monitoring and limiting the energy fed to the faulted system as quickly as possible by means of fast detection and switching-off the power supply. In DOL motor cases detection of overcurrent is often made with current transformers measuring the motor line currents. Motor is supervised by functionalities of the protection relay; if excessive motor input current or energy based on  $i^2(t)$  criterion is detected, a signal to open the circuit breaker is activated. Because of the selective protection and the time needed for reaction and opening the circuit breaker, the total time from detection of the fault condition until switching off the power supply is hundreds of milliseconds.

In case of variable speed applications, the motor is galvanically isolated from the supplying grid by a VFD. The motor is protected by the integrated VFD protection system which is based on the current measurement; in the event of short-circuit high over-current is detected resulting in a system trip, which usually takes place within milliseconds or in shorter time. Too often the short-circuit analysis for VFD supplied motors is neglected assuming that the short-circuit torque is limited by the fast reaction of the VFD and its protection functions. In both cases for DOL and VFD supplied motors, the short-circuit current and the resulting electromagnetic torque is limited solely by a short-circuit impedance of the motor. Short-circuit torque is not limited by the frequency converter, unless an additional impedance is applied in its output. Only the elapsed time after which the power supply of the faulted motor circuit is switched-off makes the difference. Therefore, short-circuit analysis is essential not only for DOL motors, but also for VFD supplier motors.

Short-circuit current and torque characteristics for a large power DOL induction motor is provided normally as a part of project documentation from the motor manufacturer. This should be the case also for the VFD applications. In addition to high transient torque levels, the high line currents during short-circuit event can cause excessive dynamic forces and heat losses. Short-circuit current characteristics are needed to dimension the power supply and set its protection features for the event of short-circuit. Therefore, it is often required to calculate or test the short-circuit withstand capability of motor components as well as main terminal boxes, power cabling, connectors and bushings. Short-circuit torque information is necessary for the mechanical assessment of the coupling and train, but especially for the rotor dynamic analysis. Analysis is required to perform based on the short-circuit excitation torque described below.



## METHODS OF DERIVATION OF TRANSIENT EXCITATION TORQUES

Transient short-circuit torque are produced within an electric motor when a fault occurs in its electrical circuit. A short-circuit fault in a power system is an abnormal condition that involves one or more phases unintentionally coming in galvanic contact with ground or between each other. During a short-circuit condition the system voltage will decay at the rate defined by the motor impedance. The rotating magnetic field in the rotor attempts to compensate the reduced voltage by becoming a power source. The magnetic energy stored within the motor causes it to act momentary as a generator; it feeds high current towards the fault resulting in a high transient torque. In case of a conventional induction motor, this phenomenon typically lasts couple of cycles. For a high-speed motor number of cycles is higher.

The determination of the short-circuit torque magnitude is a complex calculation task. Calculation methods are either analytical based on the equivalent circuit parameters or Finite Element Method (FEM) based analysis of the motor. The type of the motor, type of the fault, its location and its duration all influence on that magnitude. Analytical procedures are mostly difficult to apply to the actual case, especially for a motor utilizing a solid-rotor. This paper proposes a simple analytical calculation method based on the equivalent circuit parameters of the motor. Uncertainty in the method is in the accuracy of the equivalent circuit parameters during the transient short-circuit event.

Electromagnetic properties of an induction motor can be described in a single-phase equivalent circuit.

Figure 5 shows a typical single-phase equivalent circuit description. The parameters of the equivalent circuit allow for the calculation of motor operation characteristics and performance, including estimation for the short-circuit torque. Regardless if analytical or FEM method is selected motor characteristics such as motor phase-to-ground voltage  $U_s$ , stator resistance  $R_s$ , stator reactance  $X_s$  and rotor inductance  $X_r$  are needed to define before any calculation is possible to carry out. When FEM is utilized parameters for motor iron loss resistance  $R_m$ , magnetizing reactance  $X_m$ , and slip  $s$  dependent rotor resistance  $R_r$  are computed based on material and geometry inputs.

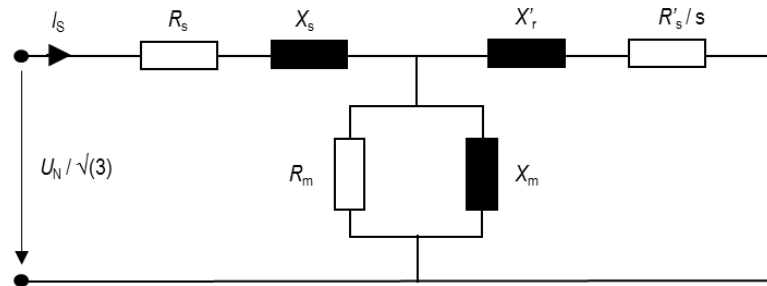


Figure 5: Single Phase Equivalent Circuit of an Induction Motor.

### Three-and Two-Phase Short-Circuit Calculations with Analytical Equations

A balanced three-phase short-circuit implies that all three phases of the power system are simultaneously short-circuited to each other through a direct connection. Equation for electromagnetic airgap torque  $T_{em,3ph}$  in case of three-phase short-circuit can be formulated from the motor torque equation. The generic for short-circuit torque equation as a function of time  $t$  can be expressed as following

$$T_{em,3ph}(t) = -\frac{3pU_s^2}{\omega_s X_s} K \sin(\omega t) e^{-\frac{t}{T}} \quad (1)$$

where  $p$  is the number of pole pairs,  $U_s$  is the motor rms phase voltage. Stator reactance  $X_s$  is a product of the angular velocity of the rotating magnetic field  $\omega_s$  and the stator inductance  $L_s$ . The motor magnetizing inductance  $L_m$ , the stator leakage inductance  $L_{\sigma s}$  and the rotor leakage inductances  $L_{\sigma r}$  are needed for the definition of the stator inductance  $L_s$ .

$$X_s = \omega_s L_s = \omega_s \left( L_{\sigma s} + \frac{L_m L_{r\sigma}}{L_m + L_{r\sigma}} \right) \quad (2)$$



The motor time constant  $T$  is a product of the stator and rotor time constants  $T_s$  and  $T_r$

$$T = T_s T_r = \frac{L_s L_r}{R_s R_r} = \frac{\left(L_{\sigma s} + \frac{L_m L_{r\sigma}}{L_m + L_{r\sigma}}\right) \left(L_{\sigma r} + \frac{L_m L_{s\sigma}}{L_m + L_{s\sigma}}\right)}{R_s R_r} \quad (3)$$

A factor  $K$ , needed in the calculation of electromagnetic torque, is defined as following

$$K = K_s K_r = \frac{L_m^2}{(L_m + L_{s\sigma})(L_m L_{r\sigma})} \quad (4)$$

Two-phase short-circuit means line-to-line short between two of the phase circuits. Difference to three-phase short-circuit is that a two-phase short-circuit produces a braking torque at the fundamental with second order frequency component. Generated electromagnetic airgap torque  $T_{em,2ph}$  as a function of time  $t$  can be expressed in form

$$T_{em,2ph}(t) = -\frac{3pU_s^2}{\omega_s X_s} K (\sin(\omega t) - 0.5 \sin(2\omega t)) e^{-\frac{t}{T}} \quad (5)$$

Both Equations (1) and (5) assume a constant rotational speed of the motor.

Figure 6 shows three- and two-phase short-circuit torques for a four-pole motor having 5.5 MW output power at 1800 rpm. Short-circuit excitation torques are calculated by utilizing Equations 1 and 5 with the following parameters:  $U_s = 3810$  V,  $R_s = 6$  m $\Omega$ ,  $L_{s\sigma} = 0.5$  mH,  $L_m = 10$  mH,  $R_r = 20$  m $\Omega$  and  $L_{r\sigma} = 1$  mH.

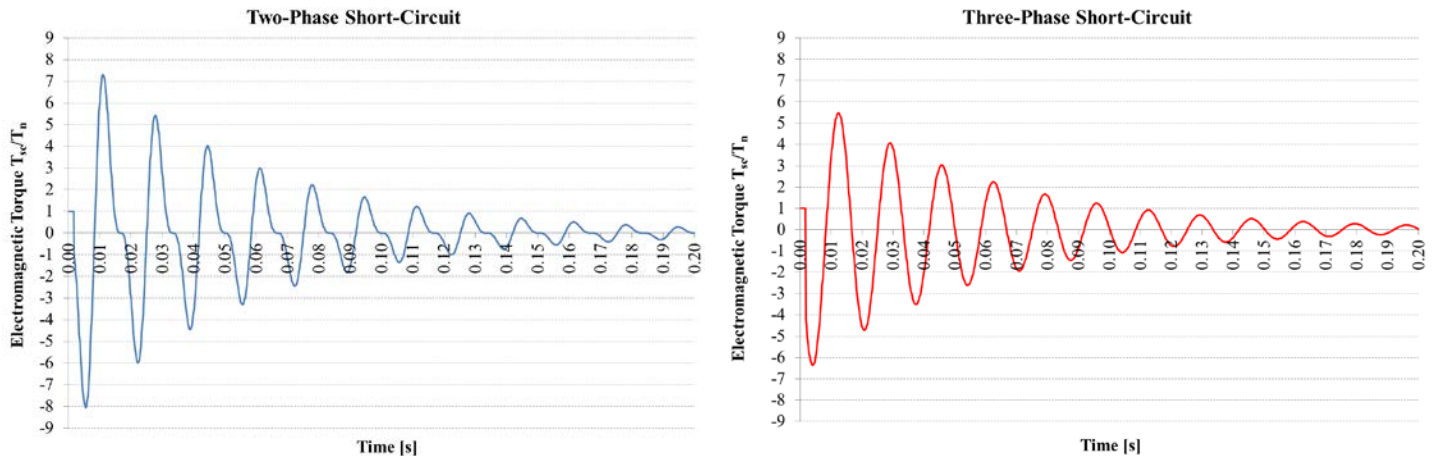


Figure 6: Two- and Three-Phase Short-Circuit Electromagnetic Torques Calculated for an Induction Motor Having Power Rating of 5.5 MW at 1800 rpm.

The exponential decay of the electromagnetic torque remains the same for both cases, two- and three-phase short-circuit calculation, as can easily be seen from Equations (1) and (5) or from the graphs in Figure 6. The calculated produced electromagnetic transient torque of decaying shape does not directly transfer to peak stress levels in distinct locations of the drive train. The reason for this is that there is considerable polar inertia in the motor rotor itself. Furthermore, torsional transient rotordynamics need to be considered, with an underlying train model with a corresponding distribution of polar inertia and local torsional stiffness values. This phenomenon is described more in detail later in this contribution. One of the practical complications is that no test method exists to verify the value of the transient excitation torque.



*Two- and Three Phase Short-Circuit Calculation with Numerical Method*

Depending on the motor design, the full set of equivalent circuit parameters or adequate analytical equations for the short-circuit torque may not be available. In such a case the calculation of the short-circuit torque by means of FEM may become necessary. FEM allows motor short-circuit torque calculations even if the equivalent circuit parameters cannot be described by the analytical equations given in the literature. One example is an induction motor with a solid-rotor; analytical calculation cannot describe the non-linear electromagnetic behavior of the rotor during the short-circuit event. FEM calculation reduces the possibility of miscalculation of rotor parameters and provides improved calculation accuracy not only for the fundamental, but also for harmonic content of the torque. In addition, compared to the analytical calculation method FEM allows easier implementation and analysis of the power supply circuit features such as asymmetries, delays in the switch-off and applying additional circuit components such as impedances. Examples for analytically and FEM calculated electromagnetic short-circuit torques for a 10 MW induction motor with a solid-rotor are shown in Figure 7. The risk of underestimating the excitation torque level for the case of short-circuits is less prone, if the results from the analytical calculations are verified with FEM calculations.

FEM calculation of two- or three-phase short-circuit torque requires always stabilized voltage-source-driven time-stepping solution. From this solution phase-to-phase voltages are calculated. The calculation of three-phase short-circuit is a straightforward task; when the three-phase short-circuit occurs, all the voltage sources are set to zero. In the case of a two-phase short-circuit one phase voltage remain healthy and the other two phase voltages have half the magnitude of the healthy value and their phase is the same. This results in one phase-to-phase voltage to be zero and the other two phase-to-phase voltages have slightly reduced magnitudes. In both cases it is important to notice that in order to take the effect of the total as well as the breaking torque into account the rotor movement must be calculated utilizing kinematic coupling. The time step size in electromagnetic FEM is must be selected low enough to maintain high resolution of the torque behavior as a function of time.

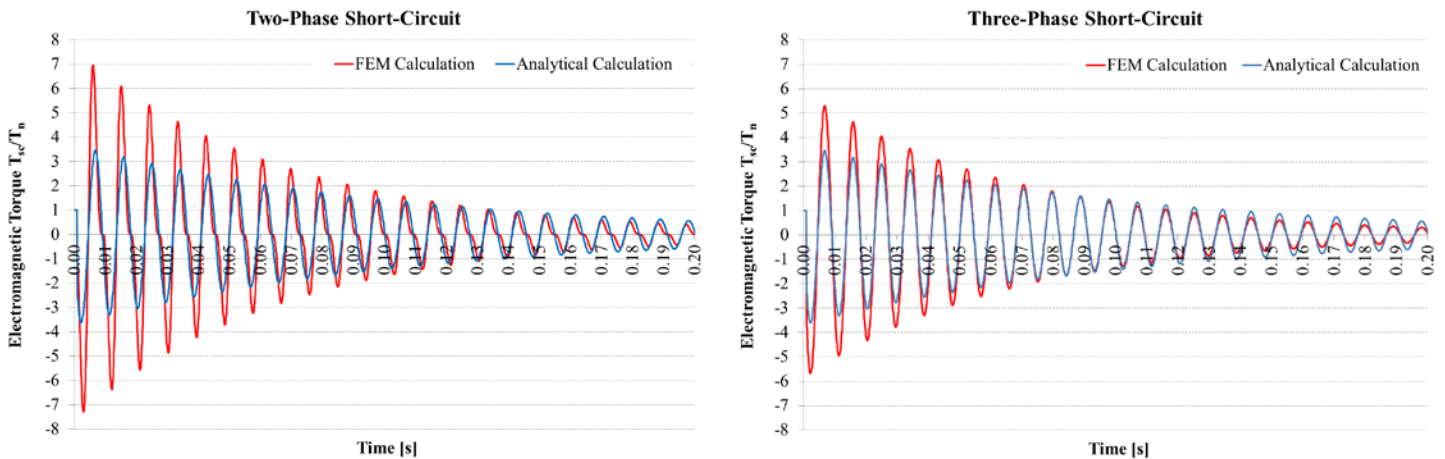


Figure 7: FEM and Analytically Calculated Two- and Three-Phase Electromagnetic Short-Circuit Torques for a 10 MW High-Speed Solid-Rotor Induction Motor.



*Two-Phase Short Circuit Followed by Three-Phase Short Circuit*

If the gate firing of the semiconductors is discontinued to stop the motor, the motor terminal voltage and current decays smoothly. Depending on the VFD features, and the severity of the fault, the VFD internal protection may either instantaneously open all the semiconductors or fire all semiconductors simultaneously. Both cases result in transient current and torque which decays at the rate defined by the motor impedance.

If all semiconductors are fired simultaneously, the motor circuit looks like all the phases are shorted at the VFD output. This means that two-phase short-circuit will be almost immediately followed by three-phase short-circuit. Unless the motor supply frequency is extremely high, the VFD will fire all semiconductors simultaneously before the short-circuit torque reaches its first transient peak. After the three-phase short-circuit is initiated due to firing of all semiconductors, a two-phase short-circuit torque will become identical to a three-phase short-circuit. FEM calculated example cases for a 10 MW two-pole high-speed induction motor are shown in the Figure 8. For these simulations, the reaction times of the VFD to fire all the semiconductors after detecting over-current were arbitrarily set to 1 ms and 5 ms which are typical value encountered. The duration after which the VFD initiates the three-phase short-circuit, and especially if it takes place before or after the first torque peak, is a relevant information in performing transient torque calculations.

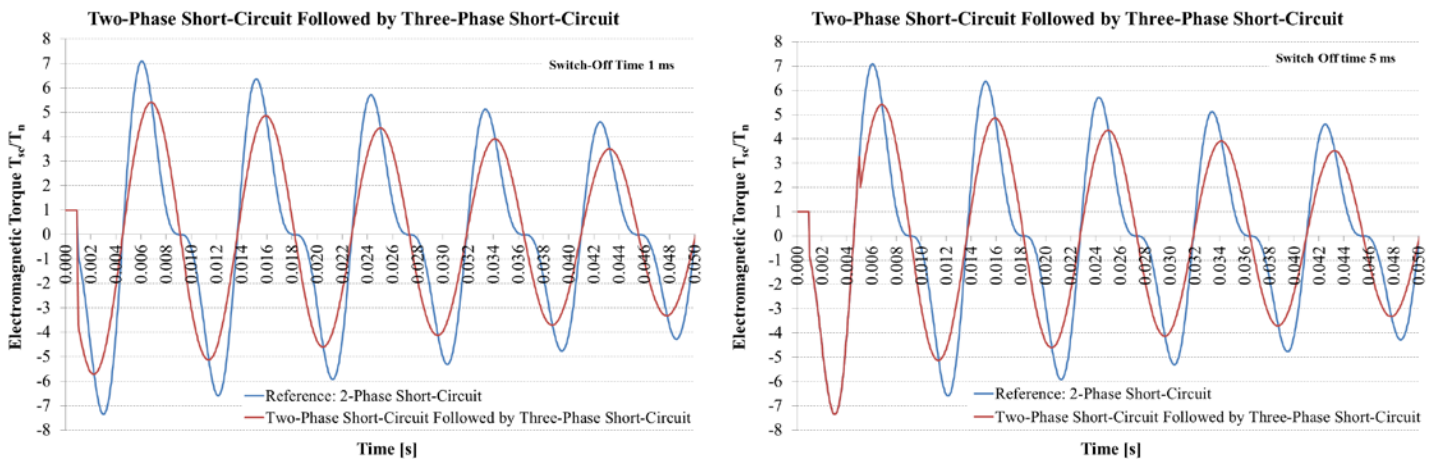


Figure 8: FEM Calculated Two-Phase Short-Circuit Torque Followed by Three-Phase Short-Circuit Initiated by VFD Protection. Calculation Was Performed for a 10 MW Solid-Rotor Induction Motor.

As it can be seen in Figure 8, when the two-phase short-circuit is followed by three-phase short-circuit, the torque waveform actually looks like the three-phase short-circuit torque. The main advantage is that the peak amplitude compared to two-phase short-circuit torque is significantly reduced and thus the stresses in the motor are smaller. Further damping of the excitation torque is possible to achieve by applying additional impedance on the VFD output.

In practice, the combination of two- and three-phase short-circuits allows to simplify the short-circuit study to be reasonably limited to the three-phase short-circuit case only. If, nevertheless, a detailed calculation for a two-phase short-circuit followed by three-phase short-circuit is required, then the use of FEM is recommended. This should ideally also be performed for different phase angles of the fundamental frequency, because it is not possible to predicted when exactly a short-circuit takes place. Especially, if the firing of all semiconductors from the VFD takes place after the first transient torque peak has been reached, calculation of the torque waveform with FEM is advisable. Of course, calculation of the electromagnetic excitation torque is possible also with analytical methods, but this requires tailored and verified analytical calculation methods. An advantage of the analytical calculation approach lies in its reduced computation cost compared to a calculation by means of FEM.



## SHORT-CIRCUIT EXCITATION TORQUE IN INDUCTION MOTORS AND ITS SENSITIVITY TO THE MAIN ELECTRIC MOTOR PARAMETERS

Electromagnetic torque is limited solely by a short-circuit impedance of the motor and therefore, the electromagnetic short-circuit torque depends strongly on the main electric motor equivalent circuit parameters as used in the equivalent circuit representation. The influence of these motor parameters on the transient excitation torque is possible to study for instance based on the Equation (1). Figure 9 shows influence of the motor equivalent circuit parameters on the short-circuit torque behavior. The actually plotted torque curves are based on the FEM simulations. Based on these torque curves it can be concluded that stator and rotor inductances both influence on the peak amplitude of the short-circuit torque; a low inductance results in a high amplitude in electromagnetic short-circuit torque. Stator and rotor resistances influence mainly on the decay of the torque; a high resistance results in a faster decay of the electromagnetic short-circuit torque.

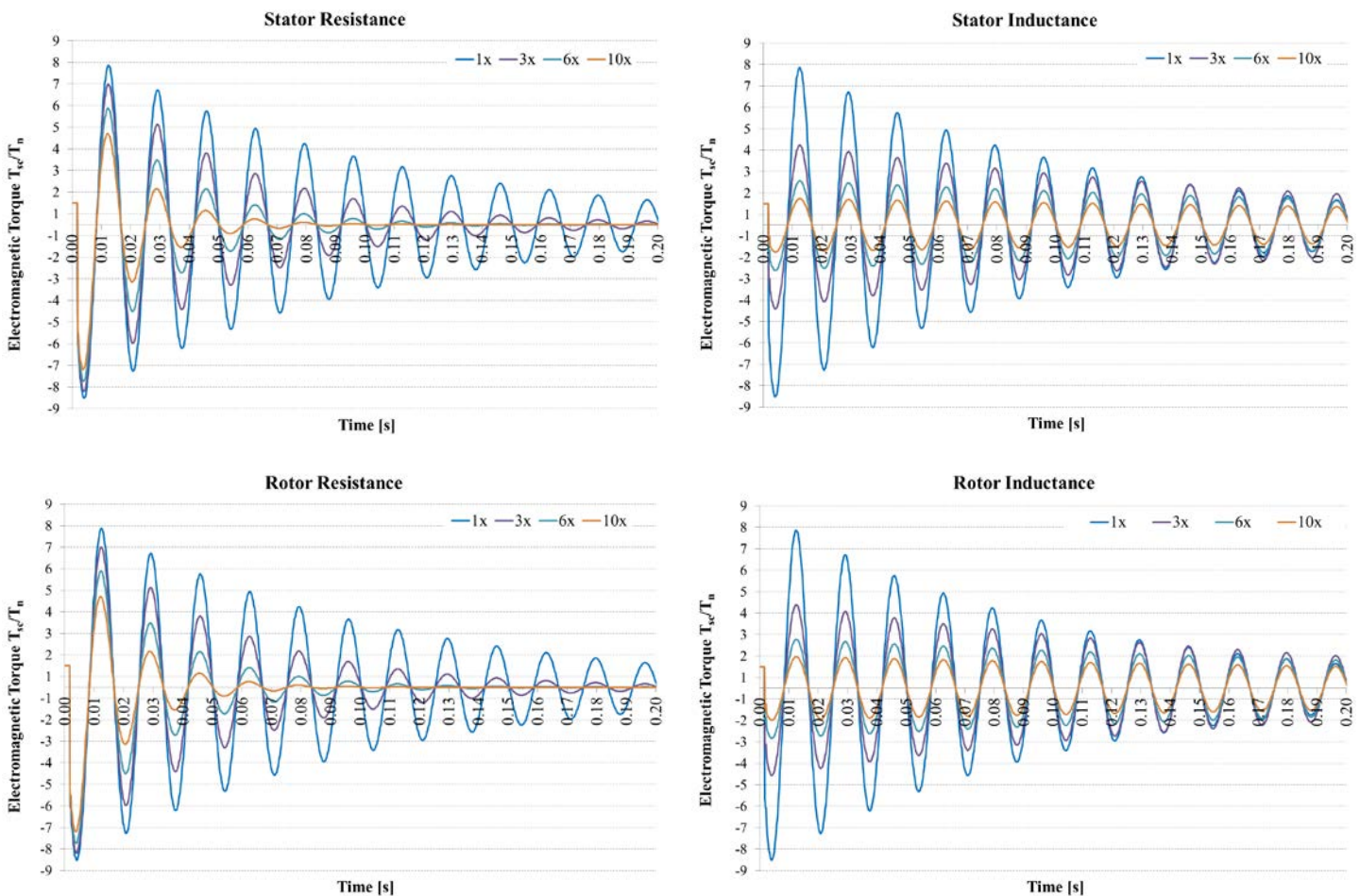


Figure 9: Electromagnetic Short-Circuit Torque as a Function of Motor Equivalent Circuit Parameters.

Equivalent circuit parameters can differ greatly for individual motor designs and it is recommended to carry out a detailed short-circuit calculation analysis if no references are available from identical motors. High-speed induction motors are mostly two-pole designs meaning that the stator inductance is typically low. This can result in relatively high short-circuit excitation torque. Typically in the conventional compressor drive trains with a speed increasing gear box the pole number of the induction motor stator is four or six. For a given rotational speed of the motor, the supply frequency needs to be increased when increasing the number of pole pairs. This can be done by the use of a VFD, however, such a motor layout leads to higher stator reactance.



### *Electromagnetic Short-Circuit Torque in Laminated and Solid Rotors*

Conventionally, electric motor rotors are made with a laminated construction with hundreds or several thousands of electrical sheets installed on the rotor shaft. Doing so may positively affect electric motor performance. However, in order to achieve higher rotor circumferential speeds or to comply with the requirements of the demanding operation environment, a solid-rotor construction is often utilized. In this paper, one area of focus is the solid-rotor construction with squirrel-cage and compared to a rotor having a laminated core. Figure 10 shows the results of calculations that were carried out for a laminated and a solid-rotor both having the same integrated squirrel-cage in the rotor and the same stator. The underlying high-speed motor has a rating of 10 MW at 6500 rpm. For the motor used in the calculations the electromagnetic short-circuit torque is higher for the solid-rotor motor. However, as explained in the earlier sections of this paper, the short-circuit characteristics can be influenced significantly by adjusting stator and rotor resistances and inductances. Further, a rotor made of one solid piece of steel is a considerably robust construction compared to other rotor structures. Therefore, judgement between these two rotor structures and technologies upon an electromechanical short-circuit behavior should not be made solely based on the Figure 10.

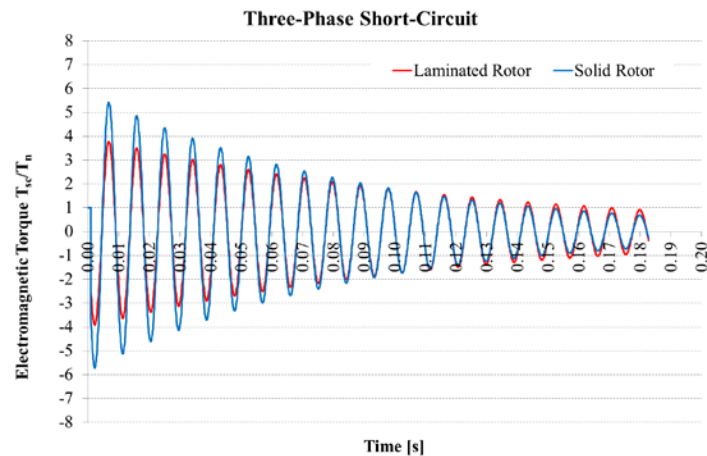


Figure 10: FEM Calculated Three-Phase Short-Circuit Electromagnetic Torque Curves for a 10 MW High-Speed Motor with Solid- and Laminated Rotors.

In a traditional laminated rotor structure magnetic field is conducted in the axially insulated electrical sheets and the torque producing axial currents are conducted in the bars of the squirrel-cage. The short-circuit impedance of the induction motor with laminated rotor structure is rather inductive. In combination with the high stator inductance that typically comes along with it the motor short-circuit currents and the resulting torque can be efficiently damped. Unfortunately it is not possible to design the electric motor by optimizing the short-circuit behavior without any trade-off concerning the motor performance during the normal operation under load.

The solid-rotor structure incorporates a rotor body made of one solid piece of steel with an integrated squirrel-cage. Different solid-rotor structures are introduced for instance by Pyrhönen et al. (2008). The solid rotor body of steel conducts both the magnetic field and the torque producing currents. This changes the main electric motor parameters for the short-circuit event significantly; during a short-circuit event the magnetic flux of the rotor is concentrated on the outer circumference of the rotor steel body resulting in low rotor inductance. In the other words, rotor impedance becomes resistive during the short-circuit event and the peak amplitude of the torque is not efficiently damped by the rotor. This is relevant as the analytical equations for the equivalent circuit parameters are not necessarily directly applicable anymore. The exemplar case described above gives a good example for the sensitivity of the rotor design upon the main electric motor parameters on the short-circuit behavior. It should be noted that it is possible to influence on the solid-rotor short-circuit resistance by materials and selections of the rotor slot size and shape. At the end the short-circuit behavior can be very similar for the laminated and solid-rotor structures.



### *Worst Case Short-Circuit Scenario*

The farther the fault is from the motor, the less pronounced will be the resultant motor excitation short-circuit torque amplitudes. This means that the worst case short-circuit is right at the motor terminals. Magnitude of the short-circuit torque caused by the stator winding insulation failure is strongly dependent on the location and voltage between the shorted coils. Therefore, an exact description of the short-circuit torque cannot be easily given for this case.

Based on the peak amplitude of the electromagnetic torque, the excitation torque in the two-phase short-circuit is the greatest. This was shown for instance in Figure 6. The case of a two-phase short-circuit containing two frequencies can be challenging from the rotor dynamical point of view because two different excitation frequency are present simultaneously in this case.

The relative time within the fundamental supply frequency (phase shift) when the short-circuit event occurs has a significant influence on the transient short-circuit torque amplitude. The worst condition is defined when the fault occurs at exactly an instant of time when the flux-linkage of one phase-to-phase voltage has its maximum value. In this paper, only the worst case has been shown and analyzed.

For VFD applications it is essential to identify the most critical motor operation points for which short-circuit and rotor torsional analysis are performed. The worst case electromagnetic short-circuit torque may not coincide with the operation with the highest power or highest speed. This is especially true, if the motor is operating in the magnetic field weakening. The highest electromagnetic short-circuit torque levels typically occur at lower than the nominal speed. By decreasing the motor supply frequency the motor impedance will lower due to a reduction in motor reactance. As the motor impedance is limiting the short-circuit torque it is inevitable that the short-circuit torque will be higher towards the lower speeds of the operation window. Table 1 shows the electromagnetic short-circuit torque peak value calculated for a solid-rotor motor having a large operation speed window.

Table 1: FEM Calculated Three-Phase Electromagnetic Short-Circuit Torque Peaks at Different Operation Speeds for a Solid-Rotor Motor Having Power Rating of 10 MW at 6500 rpm.

Rotation Speed	Electromagnetic Torque Peak $T_{sc}/T_n$
4000 rpm	7.2 pu
6500 rpm	5.9 pu
7500 rpm	5.5 pu

Motor designs with low stator impedances, high airgap flux densities, and low rotor leakage inductances are typically associated to low short-circuit impedances. This is especially true in large power high-speed two-pole induction motor designs and the resulting electromagnetic short-circuit torque levels can be extremely high.

Performing short-circuit calculations requires an understanding of various system components and their interactions. Besides the motor itself, the theoretical electromagnetic short-circuit torque depends also on other circuit components. Specifically electric capacitance can have a major influence. Additional capacitance in the motor power supplying circuit can be attributed for instance to long motor supply power cables. The special case of such is a long-step out system installed for the subsea motor-compressor, where there can be kilometers of power cables between the VFD and the motor terminals. Specific system design issues have to be addressed for combinations of high frequency and long power cables. These topics have been described for instance by (Monsen et. al, 2014).



46<sup>TH</sup> TURBOMACHINERY & 33<sup>RD</sup> PUMP SYMPOSIA  
HOUSTON, TEXAS | DECEMBER 11-14, 2017  
GEORGE R. BROWN CONVENTION CENTER

## TORSIONAL ROTOR DYNAMIC MODELLING

According to API 617 8<sup>th</sup> Ed. (2014) short-circuit calculations shall be performed and different transient excitations shall be considered e.g. two- and three-phase short-circuit cases. In the transient short circuit calculation, the induction motor's excitations resulting from two- or three-phase electrical faults as derived above are applied to the rotordynamic system. The resulting torque and stress responses are computed for each shaft element. Material damping is included in the model in order to limit the response at resonance to finite values. In order to guarantee the structural integrity of the complete shaft train, actual maximum permissible values are compared using local stresses and material stress limits. The torsional rotor-dynamic analysis is performed for two exemplary cases for the different types of compressor train configurations and their different torsional characteristics - a conventional configuration and an integrated high-speed motor compressor both using a VFD. Compressor drive train configurations are shown in Figures 2 and 3. Focus is set on the VFD driven motor trains since DOL motor trains (configuration 1) are well investigated and it is known that the torsional worst case for this kind of train configuration is normally the Start-Up load case. Nevertheless, analysis and evaluation methods presented in the following remain valid for DOL motor driven compressor trains.

### *Rotor Modelling*

For the calculation of the torsional vibrations the whole train has to be modelled. Many authors presented methods to reduce the full disk model into simple analytical lumped mass models or disk models for synchronous motor drive trains (Wachel and Szenasi 1993, Corbo and Cook 2000, Srinivasan 2011). These models are sufficient to evaluate responses of the first torsional natural frequencies and main effects can be investigated quite fast and efficient. Computation times have decreased significantly and rotor modelling has become easier with new FEM software. Complexity of train systems and therefore also the underlying number of influence parameters increase more and more for modern compressor train arrangements. FE rotor models are hence used and built up according to the rules of API 617 8<sup>th</sup> Ed. (2014), API 684 2<sup>nd</sup> Ed. (2005) and internal rules of the authors company. In Figure 11 a comparison of the respective FE rotor models of Configurations 2 and 3 is shown.



Figure 11: Comparison of the FE Rotor Models of Configuration 2 (left) and 3 (right).

### *Time Stepping and Resolution*

Applying the torsional excitations on such a rotor model yields response curves at every location of the shaft system. An example of an excitation and the respective response curve for a selected location of the shaft is shown in Figure 12. Comparing the excitation peaks with the response peaks leads to the amplification factor (AF) which is – besides the associated local stresses – the major parameter when evaluating the mechanical integrity of the train. Basically, the amplification is a measure to classify the sensitivity of the shaft system. In this paper a worst case amplification factor is identified and compared. As seen in the Figure 12, the excitation and therefore response curves are alternating in sign. Hence a maximum positive and a maximum negative value is present for both curves. For the determination of the worst case amplification factor the absolute maximum of the response peak and the absolute minimum value of the excitation peak are taken into account. In the following sections the main parameters influencing the amplification factor are discussed briefly.

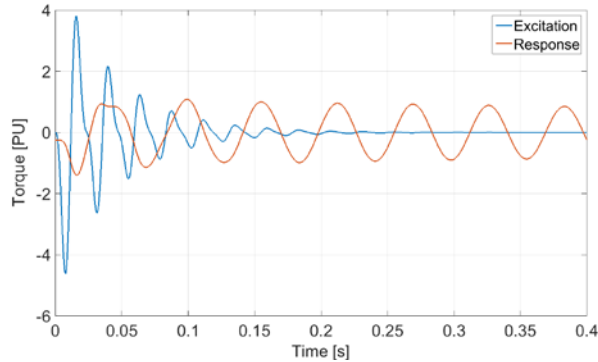


Figure 12: Example Excitation and Response Curve for a Two-Phase Short Circuit.

An important parameter is the time stepping, because it determines the resolution of the resulting torques from the torsional vibration analysis. If equations for two- or three-phase short circuits are known as function of frequency, values (mainly for laminated rotors) of Table 2 shall be used for the time step. In case that the excitation function is given as time depending load, the time stepping of the electrical calculation is recommended. If this parameter is set too coarse, the determination of response peaks can lead to significantly wrong results for the evaluation of the system. A short example of a time step variation is given in Table 3 to demonstrate the effect of wrongly chosen time stepping on the amplification factor AF.

Table 2: Recommended Time Steps for Short Circuit Calculations.

Load Case	Two-Phase SHC	Three-Phase SHC
Time step $\Delta t$	$1/(20f)$	$1/(10f)$

$f$  = rotational frequency

Table 3: Resolution Variation (Base Value: 6.5E-5s).

Time step $\Delta t$ [s]	6.5E-6	6.5E-4	6.5E-3
$\Delta$ Resulting AF [%]	0.2	34.8	846.6

### Damping

A further time dependent parameter is the duration the calculation shall cover after the excitation has decayed. Figure 12 shows that the response curve decays much slower than the excitation. An incorrect choice of the duration can lead to a significantly wrong number of load cycles and therefore to errors in the lifetime assessment. This leads to the next modelling parameter – the damping. Damping in torsional systems is practically insignificant. Except the material damping there is almost no torsional damping, with the exception of a gear (Configuration 3). A typical material damping value used is  $D = 0.625\%$ . If the train comprises a gear (Configurations 1 and 2), higher damping values can be applied depending on the train arrangement, inertia ratios and the combined lateral torsional mode shape. A detailed explanation about the determination of these values is given in Pradetto and Baumann 2015.

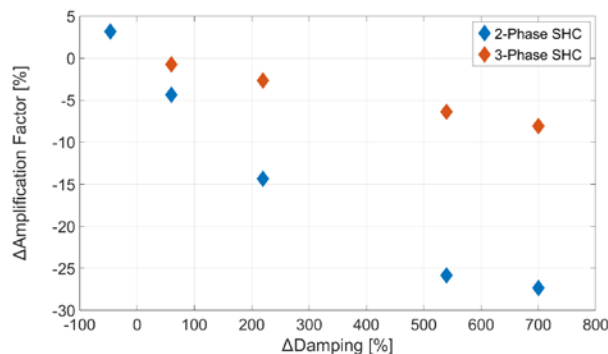


Figure 13: Damping Variation for Two- and Three-Phase Short-Circuits.



Damping really comes into play when the excitation frequency and the corresponding eigenfrequency and mode shape of the shaft coincide. An example of the damping influence on the amplification factor is shown in Figure 13; for three-phase short-circuits damping influence is minor – even an increase of damping by 700% leads to a change of about 8% in amplification factor. On the other hand, the effect of damping upon the AF is much higher for the same shaft in case of a two-phase short circuit. This is because the excitation contains a second order harmonic content that is closer to the train eigenfrequency than the first order harmonic. Hence, this shall be prevented by means of a frequency check at the start of the design phase of a new rotor using a Campbell diagram. A more detailed explanation of the use of a Campbell diagram is explained further down.

## DETERMINATION OF THE MECHANICAL INTEGRITY

As stated above, the mechanical integrity of the shaft(s) and the torque transmission components such as couplings and bolts shall be demonstrated also for short-circuit load cases. Once the load history over the time for such an event is known, determination of the mechanical integrity and the lifetime evaluation can be performed.

### *Mechanical Integrity of the Shaft*

The resulting alternating stresses should not reduce the lifetime for continuously acting stresses of any train component below allowable limits. Occurring stress peaks shall therefore not exceed the endurance limits of the used materials. Based on the strain-life theory, the Coffin-Manson equation and the assumption that distortion in these load cases is mostly elastic, tensile stress-life values are calculated based on empirical material testing. The Coffin-Manson equation can be multiplied by the Young’s modulus. By multiplying the tensile strength by the factor of 0.577 the shear tensile strength can be computed based on the von-Mises theory. The determination of the actual shear yield strength is more a complex task. The shear yield strength must be multiplied by derating factors to obtain the actual shear yield strength. These factors comprise surface effects, size effects, geometric stress concentration and additional safety factors.

The surface factor accounts for the fact that material probes are perfectly polished while real surface in the machine is not due to scratches, pits, machining marks, etc. Empirical investigations lead to surface factors in dependency of the ultimate tensile strength and the manufacturing process (Shigley and Mischke 1986). The second factor is the size factor. This factor includes the effect that the bigger the diameter of a shaft, the bigger the statistical chance that material flaw increases the material vulnerability. Since almost all torsional vibration failures occur at location of the geometric stress concentrations such as radii, keyways or shrinks, a fatigue stress concentration factor  $\beta$  has to be considered. This factor accounts for the geometric stress concentration factor  $\alpha$  and the notch sensitivity factor  $\eta$ :

$$\beta = 1 + \eta \cdot (\alpha - 1). \tag{6}$$

In a first step the geometric stress concentration factor  $\alpha$  is determined. This factor is merely dependent on geometric stress raisers and is determined by empirical tables and graphs or by means of a finite element analysis. In Figure 14 both  $\alpha$  factor determination methods are compared. A comparison for a coupling flange size series for both methods is given in Table 4. Empirical and finite element values match considerably well. An  $\alpha$  factor of 1.7 is chosen here conservatively in order to include a safety factor of approximately 1.2 for uncertainties, for example, when the actual notch radius is manufactured sharper than specified on the manufacturing drawing.

Table 4: Comparison of  $\alpha$  Factor Determination Methods: Empirical and Finite Element Method.

Flange Size normalized [%] (Outer Diameter)	126	112	100	90	80	72	64	50
<b>FEA</b>	1.43	1.47	1.42	1.45	1.41	1.44	1.42	1.47
<b>Analytical</b>	1.42	1.45	1.38	1.42	1.37	1.43	1.38	1.49
<b>Relative deviation</b>	~1%	~2%	~3%	~2%	~3%	~1%	~3%	~1%

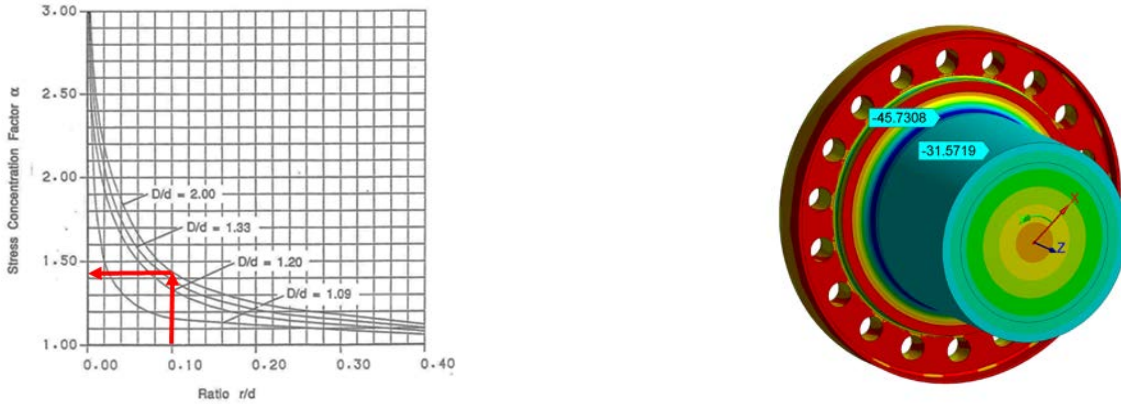


Figure 14: Comparison of  $\alpha$  Factor Determination Methods: Empirical (Peterson 1974) and Finite Element Method.

Geometric stress raiser values for bores, shrink fits, keyways etc. have to be determined accordingly. The next step is to evaluate the notch sensitivity which is a material dependent parameter. By definition it varies between 0 and 1, while 0 means a total insensitivity of the material to notches. The more ductile the material is, the lower the notch sensitivity factor is. Brittle materials have higher notch sensitivity factors, respectively. The notch sensitivity factor is determined by empirical approximations. The shear stress amplitude  $\tau_a$  multiplied by the fatigue stress concentration factor has to be limited to the shear stress endurance limit  $\tau_w$ :

$$\tau_w \leq \beta \cdot \tau_a \tag{7}$$

Because of accumulated uncertainties, such as geometry variation, surface finish, actual operational loads, damping, etc. most authors recommend an additional safety factor of 2.0. According to industry standard the weakest section of each train or shaft component (i.e. motor, compressor, gear, etc.) shall be evaluated which is usually located at the couplings, bearings or the shrink fits.

Generally, results of torsional vibration calculations are classified into following load event categories: normal operation, often occurring load events (daily event) and seldom occurring load events (100 times over the machine lifetime). For clarity see Table 5:

Table 5: Torsional Load Event Categories.

Event / Type of Excitation	Normal operation	Often Occuring	Failure Case
Load	Ripple content	Start Up, Interharmonics	Short Circuit
Evaluation/Limit	Endurance Limit	Wöhler Line 10'000	Wöhler Line 100

For often occurring load events e.g. torsional interharmonics or transients occurring during starting of DOL machines, a lifetime calculation has to be performed. In these cases the critical shaft sections are subjected to a number of different cyclic stress levels. Consequently a damage accumulation algorithm is needed in order to determine fatigue life limit. To calculate the permissible number of starts for a rotor using the Palmgren-Miner rule (Miner 1945) and the Wöhler Line is widely used. For these load cases time duration of the calculation has to be sufficient as mentioned in the previous section.

In the case of a short-circuit of a motor, where the system is only excited for a very short time and a limited number of cycles, the torque response is usually characterized by some large peaks followed by a fast decay of the amplitudes. Hence only shear loading of the shaft(s) is considered. Furthermore the torsional vibration amplitudes are significantly higher than the static torsional deflection during normal operation (1 pu). If these events are identified as the worst cases, the design of the shaft is then based on the material yield strength (Grgic et al. 1992).

In addition to the mechanical integrity check of the shaft, several other components shall be analyzed with respect to short circuit events. Peak torques occurring at the coupling have a significant effect on the integrity of the coupling bolts and shrink fits. Furthermore, other shrink fits, i.e. impeller fits, shall also be designed to withstand overload due to short-circuit torque transient torque peaks. Coupling and impeller shrink fits are checked with the method described above to verify that they are designed sufficiently. Besides material overstressing, relative motion between shaft and shrunk-on components (slip) needs to be excluded by calculation.



*Mechanical Integrity of the Coupling Bolt*

The assessment of the coupling bolts differs from the method above which only focusses on the shear stresses. Since coupling bolts are pretensioned, these parts are loaded by a combination of tensile and shear forces. There are a lot of methods and publications when it comes to determine the bolt strengths to various load cases and load combinations. At the authors' company the empirical method developed by Steeve and Wingate (2012) is used. The method is based on static experiments, but is suitable for short-circuit load events since these are quasistatic load events. Typically maximum normal stress and maximum shear stress theory is used to predict the ultimate failure of a part in combined shear and tension. For this method load factors  $R_s$  for shear loading,  $R_t$  for tensile loading and the ratio of maximum shear and maximum principal stress  $k$  are calculated:

$$R_s = \frac{\tau}{\tau_{allow,bolt}} \quad (8), \quad R_t = \frac{\sigma}{\sigma_{allow,bolt}} \quad (9) \quad \text{and} \quad k = \frac{\tau_{allow,bolt}}{\sigma_{allow,bolt}} \quad (10)$$

Using the maximum normal stress and maximum shear stress theory and setting  $k = 0.5$  the simple relation is determined:

$$R_s^2 + R_t^2 = 1 \quad (11)$$

This conservative approach is the most cited for combined shear and tension load cases. Loads are calculated for one point of the section. The failure behavior of a bolt is determined by the shear strength at the shear plane on the one hand and the tensile strength at the threads on the other hand. Since the tensile strength is lower at the thread than at the shear plane and shear and tensile failures occur at different locations of the bolt the criterion given in equation (11) is much too conservative. Steeve and Wingate (2012) did a test series to determine the relationship between shear and tensile failure modes for threaded bolts. They recommend to use the following modified failure criterion to evaluate the mechanical integrity of bolts in combined shear and tensile loading:

$$R_{s,body}^{2.5} + R_{t,thread}^{1.5} = 1. \quad (12)$$

For the bolt assessment of the investigated compressor trains the maximum torques as result of short circuit excitations are determined at the location of the bolts. The load factors  $R_{s,body,res}$  and  $R_{t,thread,res}$  are calculated and compared against the respective limit. For the calculation of tensile load factor  $R_{t,thread,res}$  bolt pretension is calculated. A lot of calculation methods exist to determine the correct values for the pretension. At this point reference is made to the VDI 2230 (2015) which gives all the necessary equations. The shear load factor  $R_{s,body,res}$  is determined by calculating shear stress in the bolt body at 1 pu and a scaling with the net torsional excitation. Net torsional excitation is the pu value resulting from torsional excitation minus the torque which is transmitted via friction. According to API 671 4<sup>th</sup> Ed. (2007) this value is at least 1.2 pu. A bolt safety factor can be calculated as the inverse value of the resultant load factor.

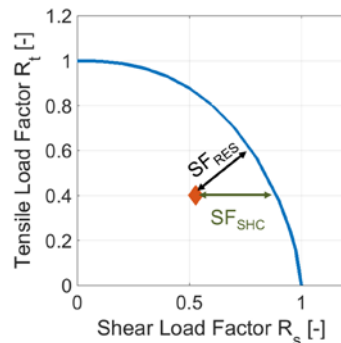


Figure 15: Resultant Load Factor

Figure 15 shows a graphical representation of the bolt assessment. Bolt safety factor and short circuit safety factor is also given. It can clearly be seen that in this case the safety factor for short-circuit is much higher than the resultant load factor. With the help of this assessment method a clever compromise between needed tensile pretension (requirements API 671 4<sup>th</sup> Ed. (2007)) and high safety factors for all relevant failure modes can be found.



## COMPARISON OF TORSIONAL TRANSIENT BEHAVIOR FOR DIFFERENT CONFIGURATIONS

In the following sections principles to identify the critical operation points from the rotor dynamics point of view are discussed. The different torsional characteristics for different types of train configurations are outlined. Methods to calculate and evaluate the fatigue limits for particular parts of the shaft system are also presented in the previous section. Beside the amplification factor, the absolute value of the response is of great interest since these values determine the mechanical integrity as presented in the previous chapter. Nevertheless the focus for the following sections is to determine the different amplification factors to discuss various design parameters.

### *Campbell Diagram and Mode Shapes*

As explained above the amplification factor is determined by the excitation given by the electrical torques on the one hand and by the response of the system on the other hand. Damping is nearly insignificant except in case of a resonance. Thus the response of the system highly depends on its eigenfrequencies (EF) and their respective mode shapes in the vicinity of the excitation frequencies. Due to the frequency content of the excitation, for three-phase short-circuits only the fundamental is critical, for two-phase short-circuits the fundamental and the 1<sup>st</sup> harmonic. It is also shown that the operating point plays an important role when it comes to the determination of the worst case. Therefore, the whole operating speed range of the motor has to be considered. For a train comprising a gear two speed areas and shafts shall be analyzed, for a high-speed train only one respectively. An exemplary Campbell Diagram of a configuration 2 train is given in Figure 16 showing the operating speed areas as well as all torsional natural frequencies in the vicinity of the operating speed. Furthermore the respective mode shapes of the first four torsional natural frequencies are given. A high response peak will occur, if the short-circuit excitation frequencies are resonant to the modes. Hence this shall be prevented in good compressor train design.

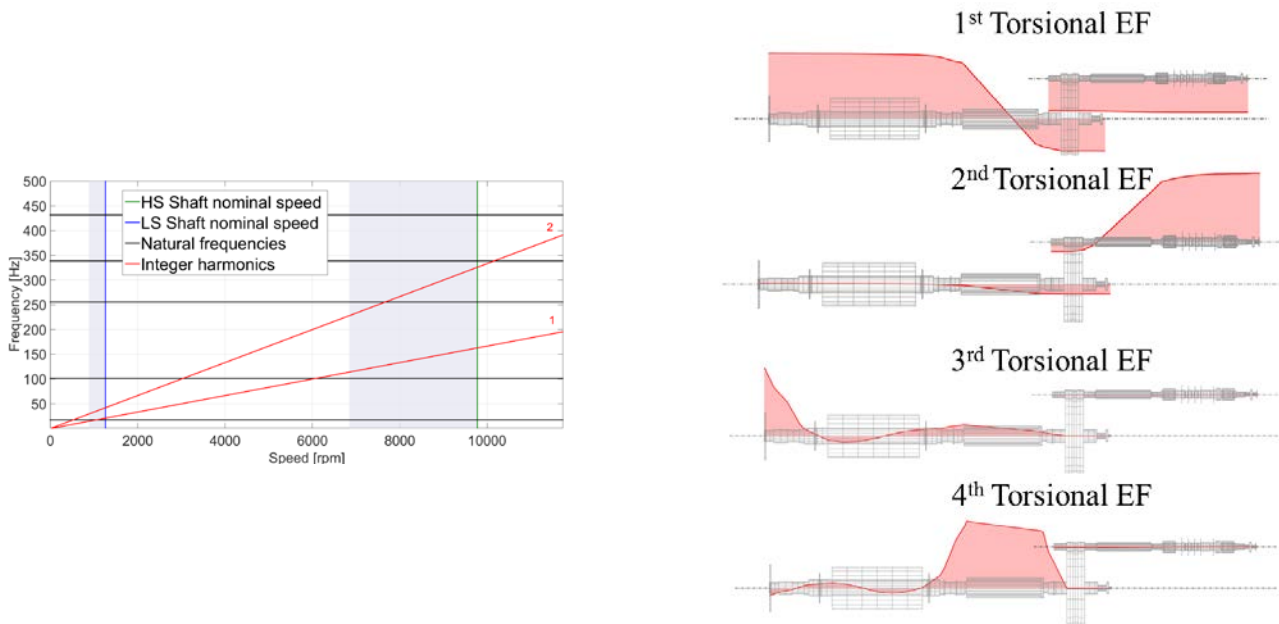


Figure 16: Exemplary Campbell Diagram of a Configuration 2 Train and Mode Shapes of the First Four Torsional Natural Frequencies (EF).

In comparison to the Campbell Diagram and Mode Shapes of a configuration 2 train, the similar graphs are given for a configuration 3 train in Figure 17. First difference catching the eye is that there is only one shaft which has to be kept free of resonances. The mode shapes of the first torsional natural frequencies are quite different due to the different designs and train arrangements of both configurations. This has to be kept in mind when it comes to the evaluation and tuning of the different configurations.



46<sup>TH</sup> TURBOMACHINERY & 33<sup>RD</sup> PUMP SYMPOSIA  
 HOUSTON, TEXAS | DECEMBER 11-14, 2017  
 GEORGE R. BROWN CONVENTION CENTER

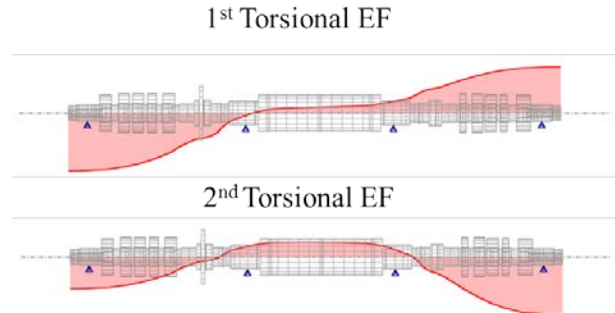
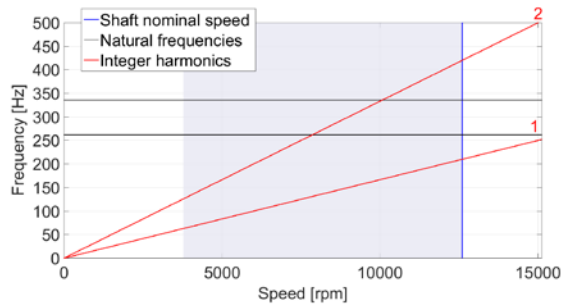


Figure 17: Exemplary Campbell Diagram of a Configuration 3 Train and Mode Shapes of the First Two Torsional Natural Frequencies.

### Shaft Shear Stresses

As described in the previous chapter shear stresses induced by short circuit excitations are calculated by the means of a FEM program. The resulting stresses are then multiplied by the respective fatigue stress concentration factor  $\beta$  (according to Equation (7)). Figure 18 shows the calculated stress response of a two-phase short circuit calculation of train configuration 3. Below the graph displaying the time history of the shear stresses for every shaft section the shaft sections are drawn. The area is colored according to the safety factor which is the inverse value of the absolute maximum of the calculated shear stresses divided by the allowable stress level. This allows a quick and easy detection of the mechanical integrity of every shaft element and the identification of the most loaded sections of the shaft. In this case the coupling area comprising also the axial bearing is the most critical section. Comparing the time at which the maximum response peak occurs at each of the compressors it can be seen that they are alternating. This is linked to the torsional natural frequency and shall be looked at in context to the mode shapes given in Figure 17.

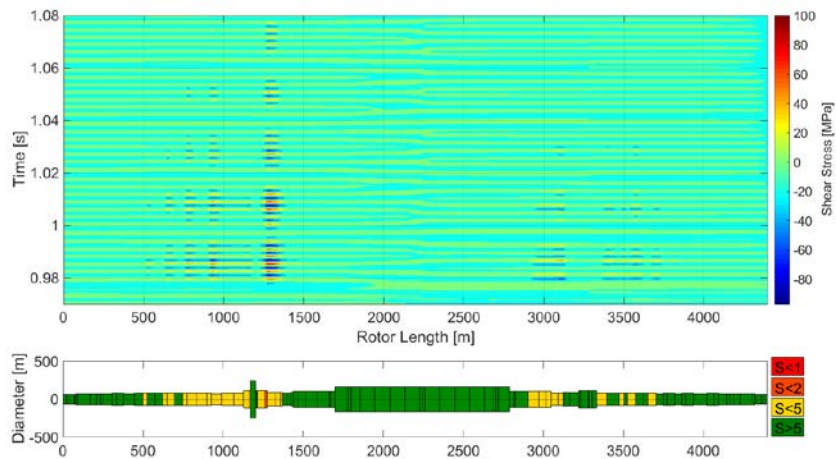


Figure 18: Torsional Shear Stress Two-Phase Short Circuit Evaluation of Configuration 3.

In analogy to the shear stress evaluation of the configuration 3, two graphs are shown in Figure 19 for the Low Speed (LS)-and High Speed (HS) shafts. For the LS shaft (motor) the most critical section is the motor shaft end. The soft LS coupling decouples the gear from any high shear stress peaks. The most critical shaft section for the HS shaft (compressor) is at the last stage and the balance piston area. The comparison of both shafts shows a lot more response peaks at the HS shaft than for the LS shaft in the same investigated time range. Reason for this is the different locations of excitation and response. While for the LS shaft excitation and response location are quite close or even the same, opposite statement is valid for the HS shaft. Both Figure 18 and Figure 19 show that it is important to analyze the whole shaft and identify the most critical section.

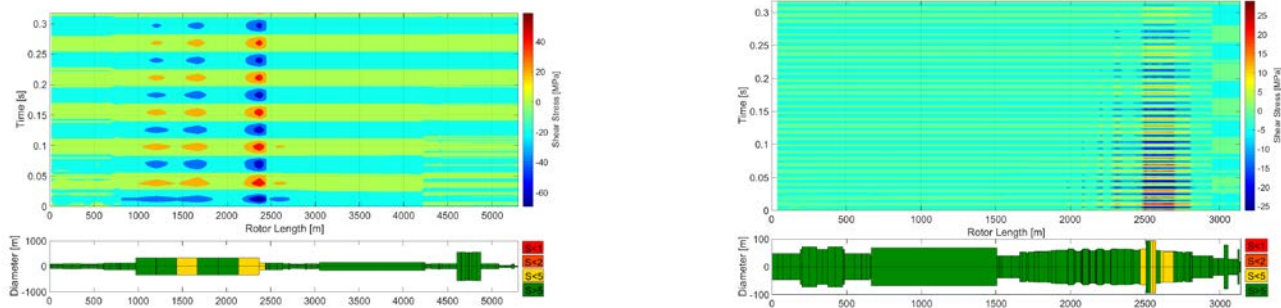


Figure 19: Torsional Shear Stress Two-Phase Short Circuit Evaluation of Configuration 2 (LS Shaft left / HS Shaft right).

### Coupling Bolts

As outlined in the previous section not only shear stresses need to be taken into account, but also the coupling bolts. The method presented is applicable for all train arrangement configurations. Main difference of configurations 2 and 3 is the number of bolt connections used. For a configuration 3 only one or two solid couplings are needed to connect the motor with the compressor(s). Therefore only two bolt locations have to be evaluated. If identical couplings are used, only the evaluation of the worst case is necessary. Configuration 2 bolt assessment is more extensive. A comparison of a flexible coupling of a configuration 2 and a solid coupling of a configuration 3 is given in Figure 20. A lot more bolts in different numbers, sizes and locations are needed to connect the LS shaft with the bull gear on the one hand and the HS shaft with the pinion on the other hand. With the highly recommended variation of bolt pretension to take pretension process uncertainties into account a lot of cases have to be investigated. Furthermore not only these facts increase the evaluation effort, but also the fact that the coupling in configuration 2 train arrangements is often an interface to another manufacturer. In industrial practice the main components of a train like couplings, motor, gearbox and compressor(s) are in the scope of different manufacturers and thus different calculation methods. Main train components of a configuration 3 train are normally in the scope of only one OEM.

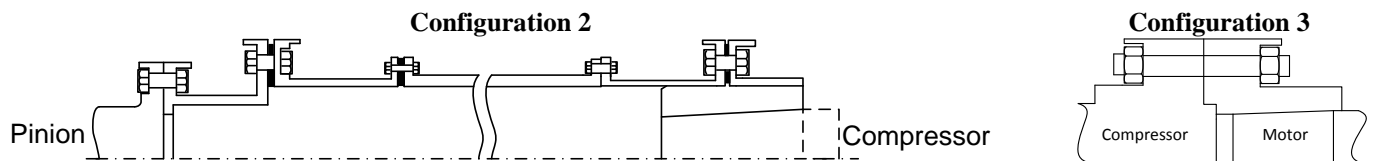


Figure 20: Scheme of a Coupling of a Configuration 2 Train and Coupling of a Configuration 3 Train.

### TORSIONAL KEY DESIGN PARAMETERS OF VFD DRIVEN TRAINS AFFECTED BY SHORT CIRCUIT

In this chapter a brief discussion on the evaluation of these systems is conducted. The main difference is that for a high-speed motor application (configuration 3) location of excitation (motor) and response (compressor) is much closer than for an arrangement comprising a gear. Responses for configuration 3 are more or less directly coupled via the coupling while transfer functions in geared trains (configuration 1 and 2) are highly influenced by the gear itself and the two couplings. The calculation and evaluation of a high-speed motor is in that context easier since a smaller number of parameters affects the results. Nonetheless there is no good or bad when it comes to find a good train design. It is merely a question of which parameters affect the torsional system behavior in case of short circuit and which components shall be looked at during the design phase.

### Tuning of the Torsional System

There are some crucial parameters which define the torsional system and its sensitivity to short circuit excitation. All torsional evaluations shall be based on a Campbell Diagram. For the first torsional eigenfrequencies enough separation margin to the respective operating speeds is strived. A high speed train arrangement (configuration 3) comprising coupling(s) to connect the high-speed motor with the compressor(s) mainly depends on the inertia ratio of motor and compressor(s). Since the inertia ratio of these components is



also an input parameter for the electrical calculation, it has to be shown that a closed loop calculation where motor excitation and compressor response are calculated in separated steps is acceptable. For the studied cases an electrical parameter study was performed using different inertia ratios. The inertia ratio is defined as inertia of the motor shaft divided by the inertia of the compressor shaft(s). The comparison given in Figure 21 shows that a closed loop calculation is suitable for the investigated cases since excitation functions and peak torques are the same for different ratios.

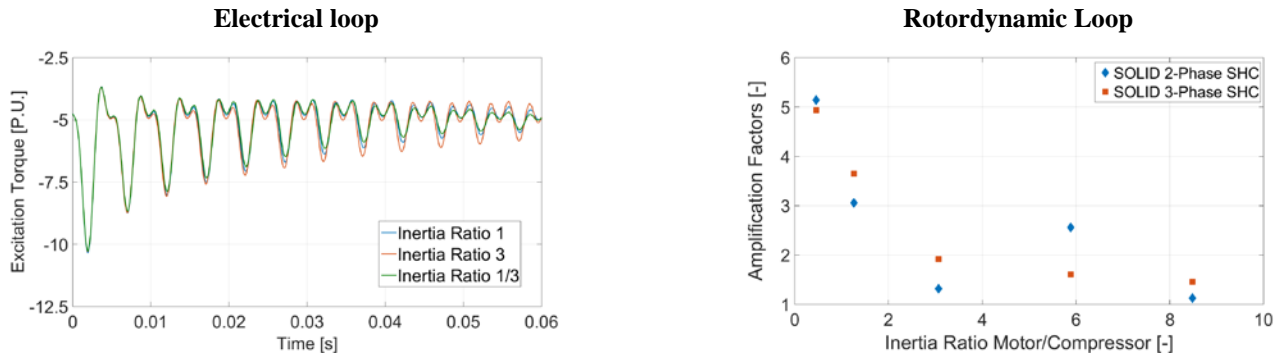


Figure 21: Comparison of Two-Phase Short Circuit Excitation Curves for different Inertia Ratios (Electrical Loop) / Effect of the Inertia Ratio Variation Configuration 3 Train comprising Solid Rotors in case of Two-Phase and Three-Phase Short Circuit on the Response (Rotordynamic Loop).

The graph in Figure 21 (right) also shows the results of a rotordynamic calculation varying the inertia ratio of motor and compressor for solid rotors in two- and three-phase short circuit for configuration 3. This confirms the basic assumption that the lower the compressor inertia the lower the response. The higher the compressor(s) inertia the higher the counteracting torque the higher the amplification. This conclusion is valid for solid as well as for laminated rotors. For the Two-Phase Short Circuit one exception exists. At an inertia ratio of 6 the response is higher than for a ratio of 3.

A look at the corresponding Campbell Diagrams reveals that in this particular case the 1<sup>st</sup> harmonic is in vicinity of the eigenfrequency which means the system is in resonance. Hence amplification is much higher for rather low compressor inertia. Figure 22 displays the spectrograph at the most critical section and clearly shows the higher amplitudes and the much slower decay of the vibration amplitudes. Furthermore it can be seen that 1<sup>st</sup> order harmonics cross the running speed which explains that only two-phase excitations lead to high amplifications (compare Figure 21).

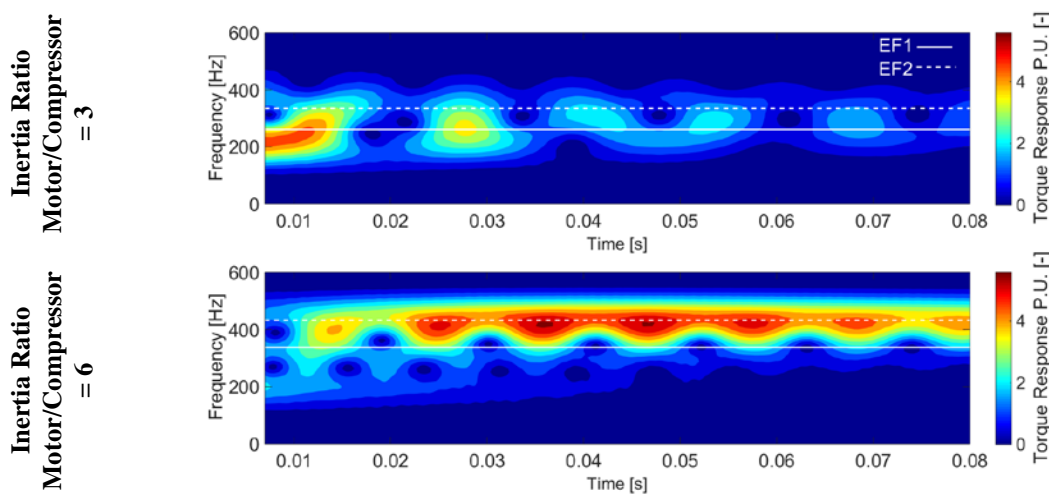


Figure 22: Spectrograph for an Inertia Ratio of 3 (top) and 6 (bottom) of a Configuration 3 Train.



As shown in the previous section inertia ratios of exciter (motor) and oscillator (compressor) determine the response of the system. For train configurations 3 this is the main influence since the shafts are coupled via solid couplings. For train configurations 1 or 2 shafts are coupled using two flexible couplings. These two flexible couplings or rather their torsional stiffness are another torsional tuning parameter which shall be looked at when designing a new train. The mode shapes of the first torsional natural frequencies representing a train configuration 2 are shown in Figure 16. Taking these mode shapes into account, it is seen that the 1<sup>st</sup> torsional eigenfrequency is mainly determined by the low speed coupling connecting the motor with the bull gear while the 2<sup>nd</sup> mode shows high deflections in the area of the high speed coupling. Hence the train system and thus its torsional signature are tunable via a variation of the stiffness of these couplings.

The graph in Figure 23 shows the effect of the low speed coupling stiffness on the resulting amplification factors and shear stresses on the left graph. In these case the higher the torsional stiffness of the LS coupling the higher the amplification factor up to a certain value, then it remains at constant high level. Comparing the progression of the amplification factor curves and the relevant torsional natural frequency (Figure 23 right) and knowing that running speed of the LS shaft is 1260 rpm the effects can be easily explained – the train is running in resonance for high LS coupling stiffness. The same trend is seen on the HS shaft, since the transfer function of the excitation remains the same. On the other hand a closer look at the safety factors of the LS shaft shear stresses shows that there is an optimum value of torsional stiffness. Values in the midrange of the investigated stiffness interval lead to the best compromise of amplification factor and shear stresses.

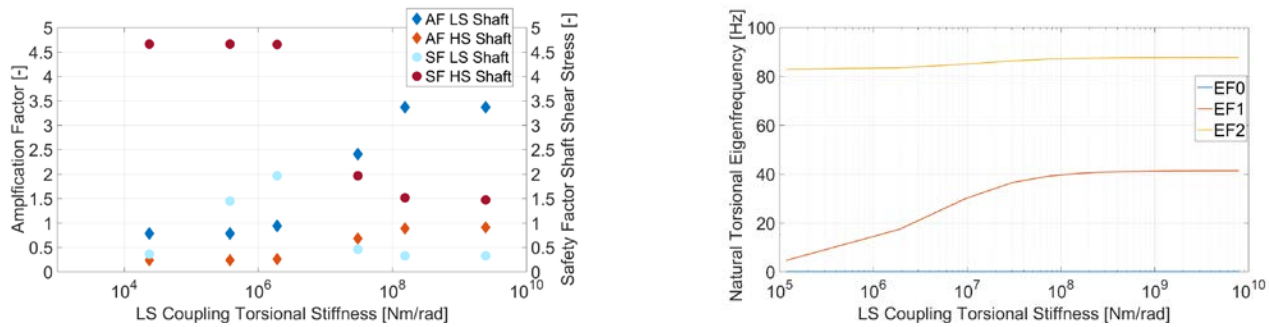


Figure 23: Effects of the LS Coupling Stiffness Variation (Configuration 2) on the resulting Amplification Factors, Shaft Shear Stresses Safety Factors (left) and Torsional Natural Frequencies (right)

### Considerations for the Shaft Design

When it comes to design a new compressor train, short circuit load cases have to be taken into account, not only because of the requirements of the API 617 8<sup>th</sup> Ed. (2014), but also these electrical faults have an impact on the mechanical integrity of the train. The first step is to determine the critical operation points. This is done by calculating the electrical excitations for different operation points of the operating area and a Campbell Diagram to analyze the systems sensitivity. Transient torsional calculations are recommended for two- and three-phase short circuits while two-phase short circuits seem to be more critical to the system because of the 2<sup>nd</sup> order excitation frequency content. For train configurations 1 and 2 a stiffness variation of the coupling stiffness is highly recommended since actual coupling stiffness is not available at the start of the design phase most of the times and a high impact on the torsional signature of the whole train. Such an analysis shows the robustness of the train with respect to torsional excitation. The same statement is valid for the inertia ratio, but less critical since inertia is mainly a function of the impellers and dry gas seals (if used) and these values are familiar to an OEM. Otherwise, looking at the system from motor manufacturers' point of view, these values affect also the motor shaft and are not that familiar. Hence the inertia ratios shall be defined for all involved parties. If not, a parameter study on the inertia ratios is also recommended. The determination of the mechanical integrity shall then be done for the whole system considering all critical sections.



46<sup>TH</sup> TURBOMACHINERY & 33<sup>RD</sup> PUMP SYMPOSIA  
HOUSTON, TEXAS | DECEMBER 11-14, 2017  
GEORGE R. BROWN CONVENTION CENTER

## CONCLUSIONS

In this paper it is shown that the short-circuit behavior of induction motors should be investigated for DOL motors, but also for VFD applications. A special focus in VFD applications is put on the high-speed motor applications. In the same way than with DOL connected motors, in VFD applications the electromagnetic short-circuit torque is limited solely by the short-circuit impedance of the motor. Short-circuit is not limited by VFD, unless an additional impedance is added in its output.

Short-circuit behavior of an induction motor in the cases of two- and three-phase short-circuits are explained. In addition, a special case in which a two-phase short-circuit is followed by a three-phase short-circuit is discussed. The duration after which the VFD initiates the short-circuit, and especially if it takes place before or after the first torque peak, is a relevant information in performing transient torque calculations.

Influence of the motor equivalent circuit parameters on the electromagnetic short-circuit torque is explained and demonstrated. Both stator and rotor resistances influence mainly the rate of decay of the transient torque. The stator and rotor inductances influence the short-circuit torque peak amplitude. Calculations for the electromagnetic short-circuit torque can be performed either utilizing analytical equations or FEM. It is recommended that the analytical calculations are verified with FEM. Specifically for the solid-rotor induction motors for the high-speed applications this is necessary.

The worst case for the short-circuit excitation torque level for VFD supplied motors does typically occur at lower than nominal speed. Proper torsional analysis of the VFD supplied motor necessitates the calculation of the motor torques through the speed range. Torsional system investigation has to be carried out in detail regarding their excitation frequencies and eigenfrequencies if no references are available from identical motors.

The electrical excitation functions have to be applied on the mechanical rotordynamic system to evaluate their impact on the mechanical integrity of the train. Hence amplification factors and eigenfrequencies shall be determined by the means of transient torsional analysis and a Campbell diagram. Depending on the train design and configuration, the system can be tuned by varying the coupling(s) stiffness and the inertia. The determination of the mechanical integrity shall be then done for the whole system considering all critical sections including all shrinks, couplings and bolt connections.



46<sup>TH</sup> TURBOMACHINERY & 33<sup>RD</sup> PUMP SYMPOSIA  
 HOUSTON, TEXAS | DECEMBER 11-14, 2017  
 GEORGE R. BROWN CONVENTION CENTER

## NOMENCLATURE

AF	= Amplification Factor	
D	= Damping	[%]
DOL	= Direct On Line	
EF	= Eigenfrequency	[Hz]
em	= Electromagnetic	
f	= (Rotational) Frequency	[Hz]
f <sub>i</sub>	= Fraction of life consumption	
FE	= Finite Element	
FEM	= Finite Element Method	
k	= ratio of maximum shear and maximum principal stress	
K	= Calculation factor	
K <sub>r</sub>	= Calculation factor for rotor	
K <sub>s</sub>	= Calculation factor for stator	
LS	= Low Speed	
L <sub>m</sub>	= Magnetizing inductance	[H]
L <sub>r</sub>	= Rotor inductance	[H]
L <sub>rσ</sub>	= Rotor leakage inductance	[H]
L <sub>s</sub>	= Stator inductance	[H]
L <sub>sσ</sub>	= Stator leakage inductance	[H]
HS	= High Speed	
m	= Number of phases	
OEM	= Original Equipment Manufacturer	
p	= Pole Pair Number	
ph	= Phase	
pu	= Proportional Unit	
rpm	= Revolutions per minute	
R <sub>s</sub>	= Stator Resistance	[Ω]
R <sub>s</sub>	= Shear Load Factor	
R <sub>s,body</sub>	= Shear Load Factor of the Bolt Body	
R <sub>s,body,res</sub>	= Resultant Shear Load Factor of the Bolt Body	
R <sub>t</sub>	= Tensile Load Factor	
R <sub>t,thread</sub>	= Tensile Load Factor of the Bolt Thread	
R <sub>t,thread,res</sub>	= Resultant Tensile Load Factor of the Bolt Thread	
R <sub>r</sub>	= Rotor Resistance	[Ω]
F	= Safety Factor	
s	= Slip	
SF <sub>RES</sub>	= Resultant Bolt Safety Factor	
SF <sub>SHC</sub>	= Short Circuit Bolt Safety Factor	
SHC	= Short Circuit	
U <sub>s</sub>	= Stator Voltage	[V]
T	= Time Constant	
T <sub>s</sub>	= Stator time constant	
T <sub>r</sub>	= Rotor time constant	
t	= initial time	[s]
VFD	= Variable Frequency Drive	
X <sub>m</sub>	= Magnetizing reactance	[Ω]
X <sub>r</sub>	= Rotor reactance	[Ω]
X <sub>s</sub>	= Stator reactance	[Ω]



46<sup>TH</sup> TURBOMACHINERY & 33<sup>RD</sup> PUMP SYMPOSIA  
HOUSTON, TEXAS | DECEMBER 11-14, 2017  
GEORGE R. BROWN CONVENTION CENTER

$\alpha$	= Geometric stress concentration factor	
$\beta$	= Fatigue stress concentration factor	
$\eta$	= Notch sensitivity factor	
$\sigma$	= Tensile stress	[MPa]
$\tau$	= Shear stress	[MPa]
$\tau_a$	= Shear stress amplitude	[MPa]
$\tau_m$	= Mean shear stress	[MPa]
$\tau_s$	= Shear stress strength	[MPa]
$\tau_w$	= Shear stress endurance limit	[MPa]
$\omega$	= Angular velocity	[rad/s]
$\omega_s$	= Angular velocity of stator	[rad/s]



46<sup>TH</sup> TURBOMACHINERY & 33<sup>RD</sup> PUMP SYMPOSIA  
HOUSTON, TEXAS | DECEMBER 11-14, 2017  
GEORGE R. BROWN CONVENTION CENTER

## REFERENCES

- Albrecht, P., Appiarius, J., McCoy, R., Owen, E., Sharma, D., 1986, Assessment of the Reliability of Motors in Utility Applications - Updated, IEEE Transactions on Energy Conversion, Vol. EC-1, Issue 1.
- Albrecht, P., Appiarius, J., McCoy, R., Owen, E., Sharma, D., 1987, Assessment of the Reliability of Motors in Utility Applications, IEEE Transactions on Energy Conversion, Vol. EC-2, Issue 3.
- API 617, 2014, Axial and Centrifugal Compressors and Expander-compressors, 8<sup>th</sup> Ed., American Petroleum Institute, Washington D.C.
- API 671, 2007, Special Purpose Couplings for Petroleum, Chemical and Gas Industry Services, 4<sup>th</sup> Ed., American Petroleum Institute, Washington D.C.
- API 684, 2005, API Standard Paragraphs – Rotordynamic Tutorial: Lateral Critical Speeds, Unbalance Response, Stability, Train Torsionals and Rotor Balancing, 2<sup>nd</sup> Ed., American Petroleum Institute, Washington D.C.
- Corbo, M. A., Cook, C. P., 2000, Torsional Vibration Analysis of Synchronous Motor Driven Turbomachinery, Proceedings of the 29<sup>th</sup> Turbomachinery Symposium, pp. 167-176.
- Corcoran, J.P., Kocur Jr., J.A., Mitsingas, M.C., 2010, Preventing Undetected Train Torsional Oscillations, Proceedings of the 39<sup>th</sup> Turbomachinery Symposium, pp. 135-146.
- Golebiowski, M., Ling, J.P.C.W., Knopf, E., Niedermayer, A., 2016, Torsional Robustness of the Combined Cycle Power Train Arrangement: Application of Statistical Methods to Accelerate Shaft-Line Design Cycles, Proceedings of the ASME Turbo Expo 2016, GT2016-57402.
- Grgic, A., Heil, W., Prenner, H., 1992, Large Converter-Fed Adjustable Speed AC Drives for Turbomachines, Proceedings of the 21<sup>st</sup> Turbomachinery Symposium, pp.103-112.
- Grigg C., Wong, P., Albrecht, P., Allan R., Bhavaraju, M., Billinton, R., Chen, Q., Fong, C., Haddad S., Kuruganty, S., Li, W., Mukerji, R., Patton, D., Rau, N., Reppen, D., Schneider, A., Shahidehpour, M., Singh, C., 1985, Report of Large Motor Reliability Survey of Industrial and Commercial Installations, Part I, IEEE Transactions on Industry Applications, Vol. IA-21, No. 4
- Grigg C., Wong, P., Albrecht, P., Allan R., Bhavaraju, M., Billinton, R., Chen, Q., Fong, C., Haddad S., Kuruganty, S., Li, W., Mukerji, R., Patton, D., Rau, N., Reppen, D., Schneider, A., Shahidehpour, M., Singh, C., 1985, Report of Large Motor Reliability Survey of Industrial and Commercial Installations, Part I, IEEE Transactions on Industry Applications, Vol. IA-21, No. 4
- Grigg C., Wong, P., Albrecht, P., Allan R., Bhavaraju, M., Billinton, R., Chen, Q., Fong, C., Haddad S., Kuruganty, S. Li, W., Mukerji, R., Patton, D., Rau, N., Reppen, D., Schneider, A., Shahidehpour, M., Singh, C., 1985, Report of Large Motor Reliability Survey of Industrial and Commercial Installations, Part III, IEEE Transactions on Industry Applications, Vol. IA-23, No. 1
- Hütten, V., Zurowski, R.M., Hilscher, M., 2008, Torsional Interharmonics Interaction Study of 75 MW Direct-Driven VSDS Motor Compressor Trains for LNG Duty, Proceedings of the 37<sup>th</sup> Turbomachinery Symposium, pp. 57-66.
- Karmakar, S., Chattopadhyay, S., Mitra, M., Sengupta, S., 2016, *Induction motor Fault Diagnosis – Approach through Current Signature Analysis*, Springer.



**46<sup>TH</sup> TURBOMACHINERY & 33<sup>RD</sup> PUMP SYMPOSIA**  
**HOUSTON, TEXAS | DECEMBER 11-14, 2017**  
**GEORGE R. BROWN CONVENTION CENTER**

- Kocur, J.A., Muench, M.G., 2011, Impact of Electrical Noise on the Torsional Response of VFD Compressor Trains, Proceedings of the First Middle East Turbomachinery Symposium.
- Miner, M.A, 1945, Cumulative Damage in Fatigue, ASME Journal of Applied Mechanics, pp. A159.-A164.
- Monsen, B, Rongve, K., Laegreid, T., Gutscher C., 2014, Asgard Subsea Compressor – Technology Qualification Testing with High-Speed Motor VSD and Very Long Step-Out Cable
- Peterson, R. E., 1974, *Stress Concentration Factors*, New York, Toronto: John Wiley& Sons.
- Pradetto, J.-C., Baumann, U., 2015, Coupled Torsional and Lateral Analysis for the Determination of the Damping of the first Torsional Mode of Synchronous Motor Driven Compressor Trains, Proceedings of the 44<sup>th</sup> Turbomachinery Symposium.
- Pyrhönen, J., Nerg, J., Kurronen, P., Lauber, U., 2008, High-Speed, 8 MW, Solid-Rotor Induction Motor for Gas Compression, Proceedings of 18<sup>th</sup> International Conference on Electrical Machines (ICEM'2008), Vilamoura, Portugal, September 6-9, 2008.
- Schijve, J., 1972, The Accumulation of fatigue damage in aircraft materials and structures, AGAR-Dograph No. 157, Zentralstelle für Luftfahrtokumentation, Munich.
- Shigley, J. E., Mischke, C.R., 1986, *Standard Handbook of Machine Design*, New York, New York: McGraw-Hill.
- Srinivasaan, A., 2011, Analytical Investigation of the Effects if Induction Motor Transients on Compressor Drive Shafts, Proceedings of the ASME Turbo Expo 2011, GT2011-45033.
- Steeve, B. E., Wingate, R.J., 2012, Aerospace Threaded Fastener Strength in Combined Shear and Tension, National Aeronautics and Space Administration, Huntsville, Alabama.
- VDI 2230 Richtlinie Blatt 1, 2015, Systematische Berechnung hochbeanspruchter Schraubenverbindungen - Zylindrische Einschraubenverbindungen, Verein Deutscher Ingenieure
- Wachel, J.C., Szenasi, Fred R., 1993, Analysis of Torsional Vibrations in Rotating Machinery, Proceedings of the 22<sup>nd</sup> Turbomachinery Symposium, pp. 127-151.